Convergence analysis of inertial lift force estimates using the finite element method

Brendan Harding[1]

(Received 6 March 2019; revised 21 May 2019)

Abstract

We conduct a convergence analysis for the estimation of inertial lift force on a spherical particle suspended in flow through a straight square duct using the finite element method. Specifically, we consider the convergence of an inertial lift force approximation with respect to a range of factors including the truncation of the domain, the resolution of the tetrahedral mesh and the boundary conditions imposed at the (truncated) ends of the domain. Additionally, we compare estimates obtained via the Lorentz reciprocal theorem with those obtained via a direct integration of fluid stress over the particle surface.

DOI:10.21914/anziamj.v60i0.14094 gives this article, © Austral. Mathematical Soc. 2019. Published July 1, 2019, as part of the Proceedings of the 18th Biennial Computational Techniques and Applications Conference . ISSN 1445-8810. (Print two pages per sheet of paper.) Copies of this article must not be made otherwise available on the internet; instead link directly to the DOI for this article.

Contents

1 Introduction

Inertial lift force is a phenomena which perturbs the motion of particles/cells suspended in fluid flow through micro-scale devices from the fluid streamlines. This is exploited in a range of medical technologies including the separation and identification of circulating tumour cells [14]. Over many decades inertial lift has been studied analytically for simple flows bounded by two walls [e.g. 7, 12, 2], but for flows in devices of practical interest it is generally necessary to compute estimates of the inertial lift force.

Many methods for estimating the inertial lift force on a particle have been developed and investigated including, but not limited to, immersed boundary finite difference methods [10], direct forcing fictitious domain methods [15, 11], spectral methods [16], and finite element methods [3]. Typically these methods are used in studies which solve the full Navier–Stokes equations

$$\rho\left(\partial\mathbf{u}/\partial t + \mathbf{u}\cdot\nabla\mathbf{u}\right) = \nabla\cdot\left[-p\mathbb{I} + \mu\left(\nabla\mathbf{u} + \nabla\mathbf{u}^{\intercal}\right)\right] - \rho\mathbf{g}\,, \quad \nabla\cdot\mathbf{u} = 0\,, \quad (1)$$

where ρ, μ, p, $\mathbf{u}$, $\mathbf{g}$ and $\mathbb{I}$ denote the fluid density, fluid viscosity, pressure field, velocity field, acceleration due to gravity and identity tensor, respectively, over a range of Reynolds numbers. We are interested in the estimation of the inertial lift force via a perturbation expansion of the Navier–Stokes with respect to the particle Reynolds number and using a variant of the Lorentz

reciprocal theorem, as described by Hood et al. [9]. While our research interest is particle migration within curved ducts [5, 6], here we investigate the simpler case of straight square ducts noting that most of the observations are transferable.

We examine various aspects affecting the convergence of the inertial lift force when approximated via the solution of several Stokes equations with the finite element method. Section 2 provides a brief account of how the inertial lift force is estimated. A more detailed derivation and explanation is provided by Hood et al. [9], only parts essential to our investigation are repeated in Section 2. Section 3 provides the results of a convergence analysis for the finite element code which was developed within the open source computing platform FEniCS [1]. Lastly, we summarise our findings and discuss aspects of the computation that could be investigated further.

2 Background

Suppose ℓ denotes the side length of a square cross-section, then, without loss of generality, we take the duct interior to be $\mathcal{D} = \{\mathbf{x} = (x, y, z) \in \mathbb{R}^3 : x, z \in [-\ell/2, \ell/2]\}$. The fluid is pumped through the duct via a (constant) pressure gradient to produce a laminar Poiseuille flow. A solid/rigid spherical particle with radius a and density $\rho_p = \rho$ is suspended in the flow inside the duct. The location of the particle's centre is denoted as $\mathbf{x}_p = (x_p, y_p, z_p)$. Necessarily one has $x_p, z_p \in [-\ell/2 + a, \ell/2 - a]$ and, without loss of generality, we assume $y_p = 0$ (at time $t = 0$). Figure 1 depicts the setup. The fluid domain is then $\mathcal{F} = \{\mathbf{x} \in \mathcal{D} : \|\mathbf{x} - \mathbf{x}_p\|_2 \geqslant a\}$. Since the particle is neutrally buoyant and the flow is pressure driven, gravity has no influence on the fluid or particle motion and is neglected. The particle has a velocity $\mathbf{u}_p = (u_p, v_p, w_p)$ such that $u_p = w_p = 0$ and $v_p = \partial y_p/\partial t$ is constant. Additionally, the particle is free to spin about its centre with (constant) angular velocity $\boldsymbol{\Omega}_p = (\Omega_{p,x}, \Omega_{p,y}, \Omega_{p,z})$ with $\Omega_{p,y} = 0$.

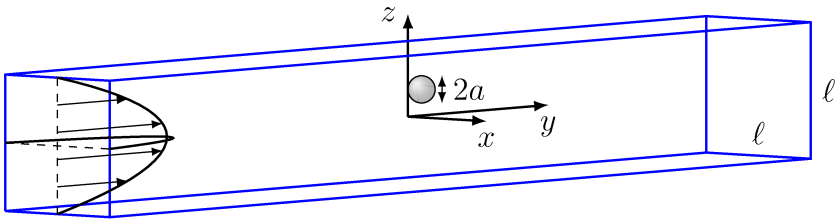

Figure 1: The setup of the duct (with axes in the centre).

It is useful to separate the fluid flow defined by the pressure and velocity fields $p, \boldsymbol{u}$ into a background flow $\bar{p}, \bar{\boldsymbol{u}}$ (defined on $\mathcal{D}$), which denotes the steady laminar flow in the absence of a particle, and a disturbance flow $q, \boldsymbol{v}$ (defined on $\mathcal{F}$), which is the difference caused by the presence of the particle. The background flow has pressure $\bar{p} = P_0 - Py$, for some constants P_0 and $P > 0$, and velocity $\bar{\boldsymbol{u}}$ satisfying $\nabla^2\bar{\boldsymbol{u}} = -(P/\mu)\boldsymbol{e}_y$ with the boundary conditions $\bar{\boldsymbol{u}} = \boldsymbol{0}$ on $\partial\mathcal{D}$. With $\bar{\boldsymbol{u}} = (\bar{u}, \bar{v}, \bar{w})$ it is straightforward to show that $\bar{u} = \bar{w} = 0$ and

$$\bar{v} = \frac{P}{\mu}\sum_{k=0}^{\infty}\frac{4\ell^2(-1)^k}{\pi^3(2k+1)^3}\cos[(2k+1)\pi x/\ell]\left(1 - \frac{\cosh((2k+1)\pi z/\ell)}{\cosh((2k+1)\pi/2)}\right).$$

It is also convenient to work in a frame of reference translating in the y direction such that the particle remains fixed. In this moving frame, the fluid domain $\mathcal{F}$ remains static/fixed and, given $\boldsymbol{u}_p, \boldsymbol{\Omega}_p$ as described above, the system is steady (such that $\partial\boldsymbol{v}/\partial t = 0$). Consequently, in this reference frame, it can be shown that $q, \boldsymbol{v}$ satisfy

$$\nabla\cdot[-q\mathbb{I} + \mu(\nabla\boldsymbol{v} + \nabla\boldsymbol{v}^\intercal)] = \rho(\boldsymbol{v} + \bar{\boldsymbol{u}} - \boldsymbol{u}_p)\cdot\nabla(\boldsymbol{v} + \bar{\boldsymbol{u}}) \quad \text{on } \mathcal{F}, \tag{2a}$$

$$\nabla\cdot\boldsymbol{v} = 0 \quad \text{on } \mathcal{F}, \tag{2b}$$

$$\boldsymbol{v} = \boldsymbol{0} \quad \text{on } \partial\mathcal{D}, \tag{2c}$$

$$\boldsymbol{v} = \boldsymbol{u}_p - \bar{\boldsymbol{u}} + \boldsymbol{\Omega}_p\times(\boldsymbol{x} - \boldsymbol{x}_p) \quad \text{on } \partial(\mathcal{D}\backslash\mathcal{F}). \tag{2d}$$

While we assume that $u_p = w_p = 0$, our goal is to estimate the hydrodynamic force on the particle in the x, z directions which ultimately leads to a non-zero (albeit small) u_p, w_p.

While the governing equations are described in a dimensional setting, it is straightforward to non-dimensionalise with the length scale a, velocity scale Ua/ℓ and pressure scale $\mu U/\ell$, where $U := \bar{v}(0)$. The right side of (2a) is then found to scale with the particle Reynolds number $Re_p = (\rho/\mu)Ua^2/\ell$ relative to the left side. When Re_p is expected to be small, rather than solve (2) directly we instead make use of a perturbation expansion such that only a few Stokes' problems need to be solved in order to approximate the inertial lift force. We continue to describe this process in a dimensional setting to avoid introducing additional notation.

Given a flow p, u on $\mathcal{F}$, the hydrodynamic force and torque on the particle are

$$F(p,u) = \int_{|x-x_p|=a} n \cdot [-pI + \mu(\nabla u + \nabla u^T)]\, dS\,,$$
$$T(p,u) = \int_{|x-x_p|=a} (x-x_p) \times \big(n \cdot [-pI + \mu(\nabla u + \nabla u^T)]\big)\, dS\,,$$

where the normal n is taken to be outward pointing from the particle centre. It can be shown that $F(\bar{p},\bar{u}) = T(\bar{p},\bar{u}) = 0$ and therefore only the disturbance flow q, v influences the particle motion. For convenience we define the mappings $\mathcal{P}(f,b)$ and $\mathcal{U}(f,b)$ which, given the vector fields f and b defined on the fluid domain $\mathcal{F}$ and particle surface $\partial(\mathcal{D}\backslash\mathcal{F})$, respectively, give the (unique) pressure and velocity fields that satisfy

$$\nabla \cdot \big(-\mathcal{P}(f,b)I + \mu\,[\nabla\mathcal{U}(f,b) + \nabla\mathcal{U}(f,b)^T]\big) = f \qquad \text{on } \mathcal{F}, \tag{3a}$$
$$\nabla \cdot \mathcal{U}(f,b) = 0 \qquad \text{on } \mathcal{F}, \tag{3b}$$
$$\mathcal{U}(f,b) = 0 \qquad \text{on } \partial\mathcal{D}, \tag{3c}$$
$$\mathcal{U}(f,b) = b \qquad \text{on } \partial(\mathcal{D}\backslash\mathcal{F}). \tag{3d}$$

We are now equipped to describe the process of estimating the inertial lift force. First one needs to solve the leading order approximation of the disturbance flow,

$$q_0, v_0 := \mathcal{P}(0,b_0), \mathcal{U}(0,b_0)\,, \quad \text{where} \quad b_0 = u_p - \bar{u} + \Omega_p \times (x - x_p)\,,$$

with the particle velocity and spin such that the system is in equilibrium, that is $\mathsf{F}(q_0, \boldsymbol{v}_0) = \mathsf{T}(q_0, \boldsymbol{v}_0) = 0$. Given the linearity of Stokes' equation, and some components of $\boldsymbol{u}_p, \boldsymbol{\Omega}_p$ being zero, the leading order approximation is solved by the following steps.

1. Solve each of $q_{0,k}, \boldsymbol{v}_{0,k} := \mathcal{P}(0, \boldsymbol{b}_{0,k}), \mathcal{U}(0, \boldsymbol{b}_{0,k})$ for $k = 1, 2, 3, 4$ where

$$\begin{aligned} \boldsymbol{b}_{0,1} &= \boldsymbol{e}_y\,, & \boldsymbol{b}_{0,2} &= \boldsymbol{e}_x \times (\boldsymbol{x} - \boldsymbol{x}_p)\,, \\ \boldsymbol{b}_{0,3} &= \boldsymbol{e}_z \times (\boldsymbol{x} - \boldsymbol{x}_p)\,, & \boldsymbol{b}_{0,4} &= \bar{\boldsymbol{u}}\,. \end{aligned}$$

2. Compute $\mathsf{F}_k := \mathsf{F}(q_{0,k}, \boldsymbol{v}_{0,k})$ and $\mathsf{T}_k := \mathsf{T}(q_{0,k}, \boldsymbol{v}_{0,k})$ for $k = 1, 2, 3, 4$ and solve the linear system

$$(\nu_p \mathsf{F}_1 + \Omega_{p,x}\mathsf{F}_2 + \Omega_{p,z}\mathsf{F}_3 - \mathsf{F}_4) \cdot \boldsymbol{e}_y = 0\,, \tag{4a}$$
$$(\nu_p \mathsf{T}_1 + \Omega_{p,x}\mathsf{T}_2 + \Omega_{p,z}\mathsf{T}_3 - \mathsf{T}_4) \cdot \boldsymbol{e}_x = 0\,, \tag{4b}$$
$$(\nu_p \mathsf{T}_1 + \Omega_{p,x}\mathsf{T}_2 + \Omega_{p,z}\mathsf{T}_3 - \mathsf{T}_4) \cdot \boldsymbol{e}_z = 0\,. \tag{4c}$$

3. Set $\boldsymbol{v}_0 = \nu_p \boldsymbol{v}_{0,1} + \Omega_{p,x}\boldsymbol{v}_{0,2} + \Omega_{p,z}\boldsymbol{v}_{0,3} - \boldsymbol{v}_{0,4}$ and similarly for q_0.

The inertial lift force is now computed by solving for the first correction to the leading order disturbance flow. Specifically, let

$$\boldsymbol{f}_1 = \rho[(\boldsymbol{v}_0 + \bar{\boldsymbol{u}} - \nu_p \boldsymbol{e}_y) \cdot \nabla \boldsymbol{v}_0 + \boldsymbol{v}_0 \cdot \nabla \bar{\boldsymbol{u}}]\,, \tag{5}$$

which is equivalent to the right side of (2a). The first correction for the disturbance flow is then

$$q_1, \boldsymbol{v}_1 := \mathcal{P}(\boldsymbol{f}_1, 0), \mathcal{U}(\boldsymbol{f}_1, 0)\,.$$

In (5) we include the term $-\nu_p \boldsymbol{e}_z \cdot \nabla \boldsymbol{v}_0$ which is absent in the derivation of Hood et al. [9] but can be found in that of Hogg [8]. The inertial lift force can be computed directly as $\mathsf{F}(q_1, \boldsymbol{v}_1)$ (noting it is the x, z components that are of principal interest). However, rather than take this direct approach, here the inertial lift force is computed without explicitly solving for $q_1, \boldsymbol{v}_1$.

In particular, let $\hat{\mathbf{u}}_x := \mathcal{U}(\mathbf{0}, \boldsymbol{e}_x)$ and $\hat{\mathbf{u}}_z := \mathcal{U}(\mathbf{0}, \boldsymbol{e}_z)$, then a variant of the Lorentz reciprocal theorem is used to show that

$$\boldsymbol{e}_x \cdot \mathbf{F}(q_1, \boldsymbol{v}_1) = -\int_{\mathcal{F}} \hat{\mathbf{u}}_x \cdot \mathbf{f}_1 \, dV, \quad \text{and} \quad \boldsymbol{e}_z \cdot \mathbf{F}(q_1, \boldsymbol{v}_1) = -\int_{\mathcal{F}} \hat{\mathbf{u}}_z \cdot \mathbf{f}_1 \, dV. \quad (6)$$

Again we refer the reader to Hood et al. [9] for further details.

This second approach may initially appear to be more effort since two Stokes' problems need to be solved (i.e. to find $\hat{\mathbf{u}}_x$ and $\hat{\mathbf{u}}_z$) as opposed to one (for $q_1, \boldsymbol{v}_1$). However, one would generally want to compute $\hat{\mathbf{u}}_x$ and $\hat{\mathbf{u}}_z$ (and the corresponding pressure fields $\hat{p}_x$, $\hat{p}_z$) regardless in order to estimate the drag coefficients on the particle in the x, z directions. For instance, these drag coefficients can then be used to determine the terminal migration velocity a particle may achieve as a result of the inertial lift force. In this context, the application of the Lorentz reciprocal theorem then provides a computational saving. Furthermore, whilst beyond the scope of this article, it is a far more convenient form to use for further analysis since linear expansions of $\boldsymbol{v}_0$ can be substituted into equation (5) and subsequently (6) to obtain a wealth of additional information about the inertial lift force at very little cost. Lastly, the results that follow demonstrate the computation of inertial lift force via the Lorentz reciprocal theorem is typically more accurate than the direct estimate.

3 Results

The standard weak formulation of Stokes' equations (3) are solved using the finite element method implemented within the open source computing platform FEniCS [1]. The domain is truncated in the y direction and two different boundary conditions are considered at the two ends: a 'natural' boundary condition which enforces zero normal stress, and a 'zero' boundary condition which enforces no-slip and no-penetration. In the latter case, the $\nabla \mathcal{U}^T$ term is dropped from the weak formulation whereas it must remain

for 'natural' boundary conditions. Conformal tetrahedral meshes of the (truncated) domain are generated using the gmsh software [4]. The mesh resolution is made to be much coarser at the ends since the disturbance flow is expected to decay away from the particle. This is a particular computational advantage from formulating the problem in terms of the disturbance flow. Taylor–Hood elements are used [13], that is first/second order Lagrange elements for the pressure/velocity spaces, respectively. The minres algorithm is used to solve the resulting linear system using an algebraic multi-grid preconditioner based on the mass matrix. In order to estimate the error in the solution (for a given mesh resolution) the same problem is solved using second/third order Lagrange elements for pressure/velocity, respectively. The solution from the lower order space is then projected into the higher order space so that the relative difference between the two can be computed.

All computations in this section consist of a particle with radius $a = 0.2$ located at $\mathbf{x}_p = (0.2, 0.0, 0.4)$ within a duct having side length $\ell = 2$. The duct is truncated at a distance 4ℓ either side of the particle (i.e. with total length $8\ell = 16$) except where convergence with respect to domain length is considered. Each mesh is non-uniform with surface elements whose edges are approximately five times smaller on the particle boundary compared to at the two ends of the duct. The relative degree of refinement, denoted here as h, is taken to be the ratio of the cube root of the average cell volume compared to those in the coarsest mesh (consisting of $\approx 1.9 \times 10^4$ tetrahedra compared to the finest mesh which has $\approx 1.6 \times 10^6$ tetrahedra).

We begin by examining mesh convergence with 'zero' boundary conditions at the ends of the duct (results were similar for 'natural' boundary conditions and are omitted). Figure 2(a) shows the relative convergence in $q_0, \boldsymbol{\nu}_0$ as solid green and blue lines, respectively. The dashed green and blue lines show the slope of h^2 and h^3, respectively and demonstrate that convergence in $q_0, \boldsymbol{\nu}_0$ is second and third order, respectively, as expected for linear and quadratic elements. Observe that $\boldsymbol{\nu}_0$ is reasonably accurate even on the coarsest mesh.

Figure 2(b) shows the relative convergence of $\mathbf{F}_4 \cdot \boldsymbol{e}_y$, $\mathbf{T}_4 \cdot \boldsymbol{e}_x$ and $\mathbf{T}_4 \cdot \boldsymbol{e}_z$ in

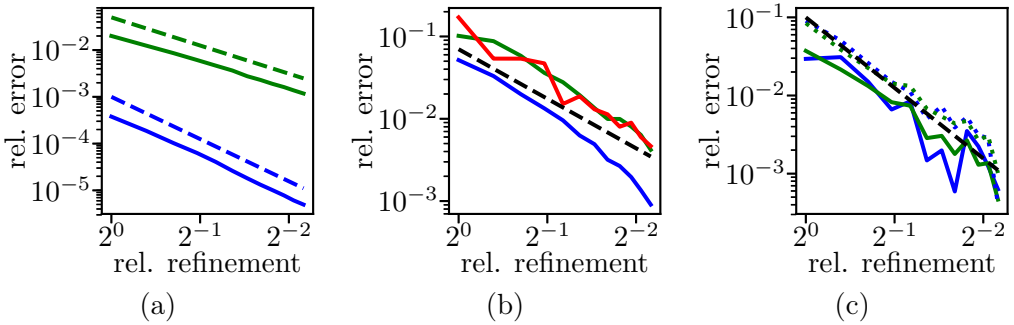

Figure 2: Mesh convergence in: (a) the leading order disturbance flow solution $\mathbf{q}_0, \boldsymbol{\nu}_0$; (b) representative force and torque coefficients that determine the spin and velocity of the particle; and (c) the x, z components of the inertial lift force on the particle. See text for further details.

blue, green and red, respectively. These are representative of the coefficients that are used to determine the velocity and spin of the particle in equation (4). Because force and torque coefficients depend on the pressure, it is reasonable to expect h^2 convergence, as indicated by the dashed black line, and the results seem consistent with this, if not slightly better.

Figure 2(c) shows the relative convergence of the x, z components of the inertial lift force in blue and green, respectively. The solid and dotted lines are the results of the reciprocal and direct calculations, respectively. The dashed black line has slope h^3 and seems to be a reasonable fit. This is somewhat surprising because of the dependence of the inertial lift on the gradient of the velocity field $\boldsymbol{\nu}_0$ which leads one to expect convergence at the rate h^2. Note that the reciprocal result is generally more accurate than the direct result. The error of both calculations is less than 1% for meshes with approximately 1.5×10^5 tetrahedra or more. There is some noise in the reciprocal result on the finer meshes which we expect is due to the finite accuracy of our estimate of the inertial lift force on the finest mesh.

The main difference due to the choice of boundary condition was observed

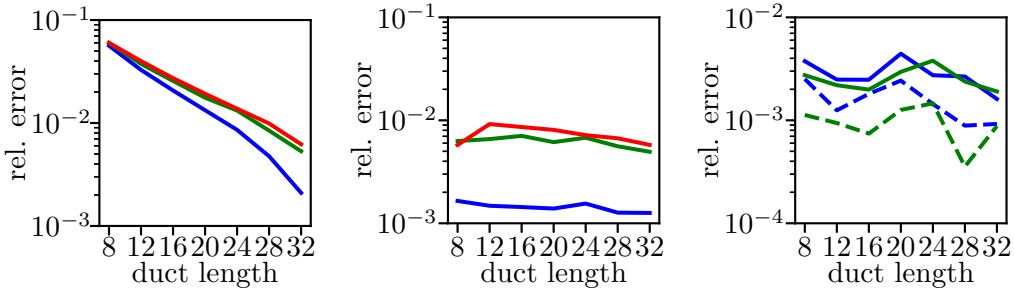

Figure 3: Convergence with respect to duct length for: (a) drag and torque coefficients in the case of 'natural' boundary conditions; (b) drag and torque coefficients in the case of 'zero' boundary conditions; and (c) inertial lift force estimates in the case of 'zero' boundary conditions. See text for details.

in examining convergence with respect to duct length. The drag coefficient in the $\mathfrak{y}$ direction is especially affected. In the case of 'natural' boundary conditions the solution $\mathfrak{U}(\mathfrak{0}, \boldsymbol{e}_{\mathfrak{y}})$ does not completely decay at the ends since the imposed motion of the particle drags a small volume of liquid through the duct with it. In contrast, this cannot occur when no-slip/penetration is enforced at the ends, and ultimately results in a larger drag coefficient.

Figure 3(a) shows the relative convergence of each of $\mathbf{F}_4 \cdot \boldsymbol{e}_{\mathfrak{y}}$, $\mathbf{T}_4 \cdot \boldsymbol{e}_{\mathfrak{x}}$ and $\mathbf{T}_4 \cdot \boldsymbol{e}_{\mathfrak{z}}$ in blue, green and red, respectively, with respect to duct length in the case of 'natural' boundary conditions. The (local) mesh resolution was not changed as the duct length increased so that longer ducts contain additional tetrahedra and the convergence primarily reflects the duct length. Interestingly, we observe that since both $\mathbf{F}_1 \cdot \boldsymbol{e}_{\mathfrak{y}}$ and $\mathbf{F}_4 \cdot \boldsymbol{e}_{\mathfrak{y}}$ are effected in a similar way, the resulting particle velocity $\mathfrak{v}_{\mathfrak{p}}$ obtained via (4) remains accurate independent of the duct length (up to mesh resolution).

In contrast to Figure 3(a), Figure 3(b) shows no convergence in the same coefficients when 'zero' boundary conditions are applied. However, the 'zero' boundary conditions results are more accurate to begin with and are essentially

already converged up to the given mesh resolution. Furthermore, we find that the resulting inertial lift estimates do not vary significantly. This is evident in Figure 3(c) which shows the x, z components of the inertial lift force in blue and green, respectively, with solid and dotted lines denoting the result of the reciprocal and direct calculations, respectively. This suggests that much shorter duct lengths can be used in the case of 'zero' boundary conditions without losing accuracy.

4 Conclusions

We examined the convergence of a finite element code for estimating inertial lift forces with respect to mesh resolution, duct length and boundary conditions. From these results we conclude that imposing 'zero' boundary conditions on the ends and using the reciprocal equation to estimate the inertial lift force is the most robust approach. Going forward we could further optimise the local size/distribution of tetrahedra over the domain, potentially via an analysis of the adjoint problem. The use of periodic boundary conditions at the ends could also be considered. An evaluation of the validity of the perturbation approximation to the inertial lift force with respect to $\mathrm{Re_p}$ would also be valuable.

Acknowledgements Computations were carried out using supercomputing resources provided by the Phoenix HPC service at the University of Adelaide. This research was supported under the Australian Research Council's Discovery Projects funding scheme (project number DP160102021).

References

[1] M. S. Alnaes et al. "The FEniCS Project Version 1.5". In: *Arch. Numer. Software* 3.100 (2015), pp. 9–23. DOI: 10.11588/ans.2015.100.20553 (cit. on pp. C67, C71).

[2] E. S. Asmolov. "The inertial lift on a spherical particle in a plane Poiseuille flow at large channel Reynolds number". In: *J. Fluid Mech.* 381 (1999), pp. 63–87. DOI: 10.1017/S0022112098003474 (cit. on p. C66).

[3] D. Di Carlo. "Inertial microfluidics". In: *Lab Chip* 21 (2009), pp. 3038–3046. DOI: 10.1039/B912547G (cit. on p. C66).

[4] C. Geuzaine and J.-F. Remacle. "Gmsh: A 3-D finite element mesh generator with built-in pre- and post-processing facilities". In: *Int. J. Numer. Meth. Eng.* 79.11 (2009), pp. 1309–1331. DOI: 10.1002/nme.2579 (cit. on p. C72).

[5] B. Harding. "A study of inertial particle focusing in curved microfluidic ducts with large bend radius and low flow rate". In: *Proc. 21st Australasian Fluid Mechanics Conference*. 603. 2018. URL: https://people.eng.unimelb.edu.au/imarusic/proceedings/21/Contribution_603_final.pdf (cit. on p. C67).

[6] B. Harding, Y. M. Stokes, and A. L. Bertozzi. "Effect of inertial lift on a spherical particle suspended in flow through a curved duct". In: *J. Fluid Mech.* (accepted, 2019). URL: https://arxiv.org/abs/1902.06848 (cit. on p. C67).

[7] B. P. Ho and L. G. Leal. "Inertial migration of rigid spheres in two-dimensional unidirectional flows". In: *J. Fluid Mech.* 65.2 (1974), pp. 365–400. DOI: 10.1017/S0022112074001431 (cit. on p. C66).

[8] A. J. Hogg. "The inertial migration of non-neutrally buoyant spherical particles in two-dimensional shear flows". In: *J. Fluid Mech.* 272 (1994), pp. 285–318. DOI: 10.1017/S0022112094004477 (cit. on p. C70).

[9] K. Hood, S. Lee, and M. Roper. "Inertial migration of a rigid sphere in three-dimensional Poiseuille flow". In: *J. Fluid Mech.* 765 (2015), pp. 452–479. DOI: 10.1017/jfm.2014.739 (cit. on pp. C67, C70, C71).

[10] N. Nakagawa, T. Yabu, R. Otomo, A. Kase, M. Makino, T. Itano, and M. Sugihara-Seki. "Inertial migration of a spherical particle in laminar square channel flows from low to high Reynolds numbers". In: *J. Fluid Mech.* 779 (2015), pp. 776–793. DOI: 10.1017/jfm.2015.456 (cit. on p. C66).

[11] T.-W. Pan and R. Glowinski. "Direct simulation of the motion of neutrally buoyant balls in a three-dimensional Poiseuille flow". In: *C. R. Mécanique* 333.12 (2005). Fluid-solid interactions: modeling, simulation, bio-mechanical applications, pp. 884–895. DOI: 10.1016/j.crme.2005.10.006 (cit. on p. C66).

[12] J. A. Schonberg and E. J. Hinch. "Inertial migration of a sphere in Poiseuille flow". In: *J. Fluid Mech.* 203 (1989), pp. 517–524. DOI: 10.1017/S0022112089001564 (cit. on p. C66).

[13] C. Taylor and P. Hood. "A numerical solution of the Navier-Stokes equations using the finite element technique". In: *Comput. Fluids* 1.1 (1973), pp. 73–100. DOI: 10.1016/0045-7930(73)90027-3 (cit. on p. C72).

[14] M. E. Warkiani et al. "Slanted spiral microfluidics for the ultra-fast, label-free isolation of circulating tumor cells". In: *Lab Chip* 1 (2014), pp. 128–137. DOI: 10.1039/C3LC50617G (cit. on p. C66).

[15] B. H. Yang, J. Wang, D. D. Joseph, H. H. Hu, T.-W. Pan, and R. Glowinski. "Migration of a sphere in tube flow". In: *J. Fluid Mech.* 540 (2005), pp. 109–131. DOI: 10.1017/S0022112005005677 (cit. on p. C66).

[16] L. Zeng, S. Balachandar, and P. Fischer. "Wall-induced forces on a rigid sphere at finite Reynolds number". In: *J. Fluid Mech.* 536 (2005), pp. 1–25. DOI: 10.1017/S0022112005004738 (cit. on p. C66).

Author address

1. **Brendan Harding**, School of Mathematical Sciences, The University of Adelaide, South Australia 5005, Australia.
mailto:brendan.harding@adelaide.edu.au
orcid:0000-0002-6755-9998